Steel and Composite Structures, *Vol. 32, No. 1 (2019) 111-126*
DOI: https://doi.org/10.12989/scs.2019.32.1.111

Static behavior of novel RCS through-column-type joint: Experimental and numerical study

Xuan Huy Nguyen [*1], Dang Dung Le [1a] and Quang-Huy Nguyen [2b]

[1] *Faculty of Construction Engineering, University of Transport and Communications, Vietnam*
[2] *Department of Civil Engineering and Urban Planning, INSA de Rennes, France*

(*Received September 29, 2018, Revised April 12, 2019, Accepted May 28, 2019*)

Abstract. This paper deals with experimental investigation and modeling of the static behavior of a novel RCS beam-column exterior joint. The studied joint detail is a through-column type in which an H steel profile totally embedded inside RC column is directly welded to the steel beam. The H steel profile was covered by two supplementary plates in the joint area in order to avoid the stirrups resisting shear in the joint area. Two full-scale through-column-type RCS joints were tested under static loading. The objectives of the tests were to examine the connection performance and to highlight the contribution of two supplementary plates on the shear resistance of the joint. A reliable nonlinear 3D finite element model was developed using ABAQUS software to predict the response and behavior of the studied RCS joint. An extensive parametric study was performed to investigate the influences of the stirrups, the encased profile length and supplementary plate length on the behavior of the studied RCS joint.

Keywords: beam-column connection; RCS joint; FE modeling

1. Introduction

Nowadays, hybrid RCS frames consisting of reinforced concrete (RC) column and steel (S) have been used frequently in practice for mid- to high-rise buildings. RCS frames possess several advantages from structural, economical and construction view points compared to either traditional RC or steel frames (Noguchi and Kim 1998, Li *et al*. 2011, Mohammad *et al*. 2013, Men *et al*. 2015a, Hui *et al*. 2018). As described by Griffis (1986), RCS frames effectively combine structural steel and reinforced concrete members to their best advantage. Several types of RCS or hybrid systems have been developed (Baba and Nishimura 2000, Cheng and Chen 2005, Fargier-Gabaldon 2005, Men *et al*. 2015b, Li *et al*. 2012, Saeedeh *et al*. 2016). One of the popular RCS system consist in first erecting a steel skeleton, which ease the realization of different construction tasks along the height of the building. RC columns are approximately 10 times more cost-effective than steel columns in terms of axial strength and stiffness (Sheikh *et al*. 1987). RC columns also offer superior damping properties to a structure, especially in tall buildings. In addition, steel floor systems are significantly lighter compared to RC floor systems, leading to substantial reductions in the weight of the building, foundation costs, and inertial forces. Due to the advantages offered by RCS frame systems, a large number of research programs have been conducted in US and Japan to study the interaction between steel and concrete members in RCS frames (Deierlein and Noguchi 2004). A primary challenge in design of RCS frames is the connection between steel beam and RC column. Indeed, using RC instead of structural steel as columns can result in substantial savings in material cost and an increase in the structural damping and lateral stiffness of the building. Energy dissipation capacity can accordingly be provided through steel beams. In an attempt to identify the in-plane behaviour of composite RCS beam-column joint connections, a comprehensive testing program was conducted at the University of Texas at Austin (Sheikh *et al*. 1989, Deierlein *et al*. 1989). 15 two-third scale interior RCS connections with various joint details were tested under monotonic and cyclic loading. From these research work, design guidelines for both interior and exterior RCS joints in buildings located in low to moderate seismic risk zones were developed by the American Society of Civil Engineers (ASCE Task Committee 1994). This research was extended by Kanno and Deierlein (1993) who tested a series of 19 interior RCS joint specimens subjected to cyclic loading. The test objective was to investigate joint failure modes, the performance of high strength concrete joints, joint aspect ratio, the effect of column axial load on the joint. Various joint details were studied, included face bearing plates, extended face bearing plates, steel columns, band plates wrapping around the columns regions just above and below steel beams, and the shear studs vertical joint reinforcement. Experimental data showed that joint details had a direct influence on the joint strength and ductility, but did not affect the overall stiffness of the specimen. In a review of ASCE Guidelines, Kanno and Deierlein (1996) cited several areas where the ASCE Guidelines could be improved. Based on the results from

*Corresponding author, Associate Professor,
E-mail: nguyenxuanhuy@utc.edu.vn
[a] Ph.D. Student
[b] Associate Professor

http://www.techno-press.org/?journal=scs&subpage=6
ISSN: 1229-9367 (Print), 1598-6233 (Online)

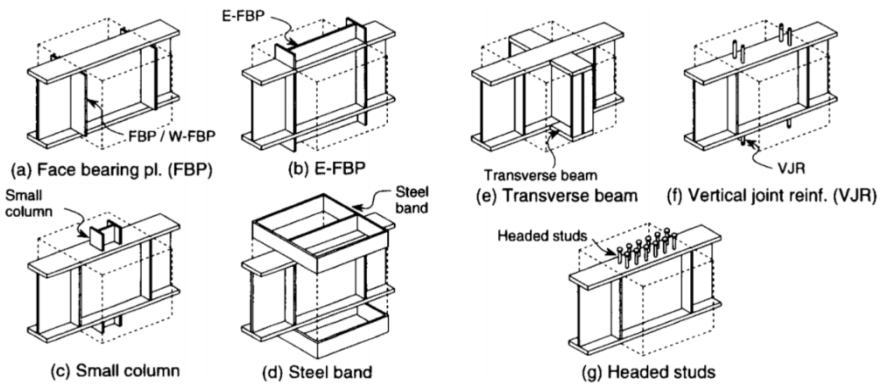

Fig. 1 Joint details considered in Kanno and Deierlein (2002) model

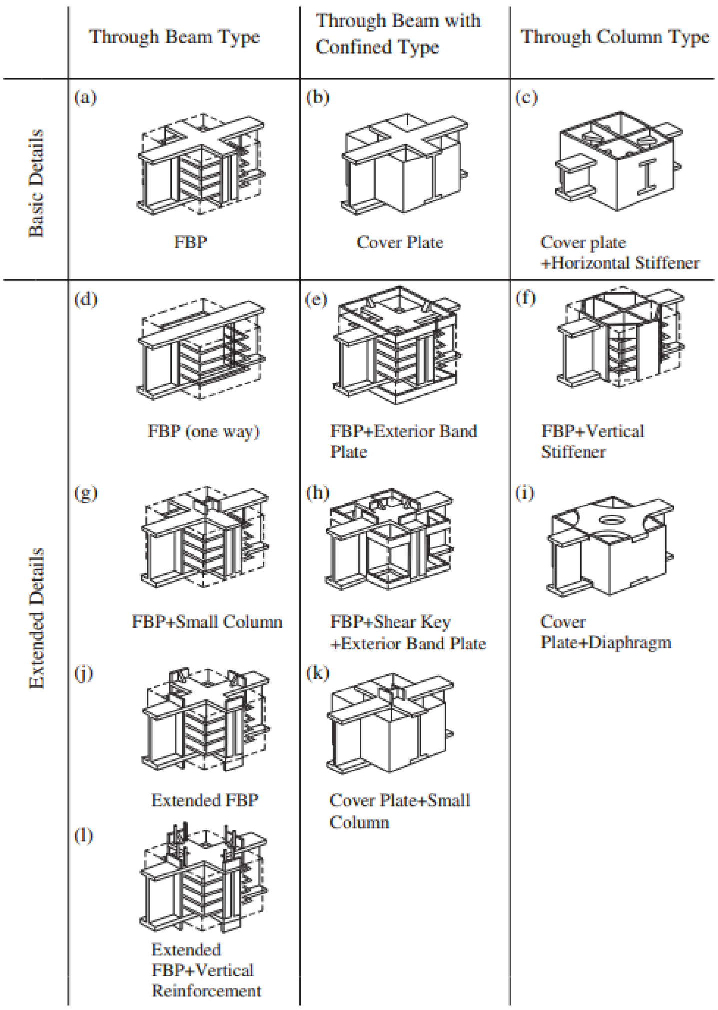

Fig. 2 Joint details by Nishiyama *et al*. (2004)

forty-four data, they reported that the joint strength model in the ASCE Guidelines was somewhat over-conservative and there was room to improve its accuracy, especially for bearing failure condition. Conservatism evident in the comparison was due in part to the fact that the ASCE Guidelines did not recognize some of the strength and stiffness enhancements provided by certain joint details. Kanno and Deierlein (2002) proposed a refined and more accurate design model for RCS joints of which the configurations are in Fig. 1. The RCS joints considered by Kanno and Deierlein (2002) are referred to as "through-beam type" details since the steel beam runs continuous through the column.

During the past two decades, a large number of RCS joint details has been proposed. This makes the applicability of RCS construction difficult since design recommendations need to be available for each joint detail (Bahman *et al*. 2012). In 2004, Nishiyama *et al*. (2004) have developed a design guide "Guidelines: Steel-Concrete Composite Structures for Seismic Design". The guidelines are proper to apply for ordinary RCS buildings, structural system comprising relatively regular-shaped frame, with or without multi-storey reinforced concrete shear walls; the height is not more than 60 m, design strength of concrete ranging from 21 to 60 MPa; and reinforcing bars and structural steel standardized in the Japan Industrial Standards. The design rule follows the "strong column-weak beam" philosophy. The joint failure modes are similar to the design guidelines of the ASCE 1994, for the shear failure and bearing failure. The joint details treated in the Guidelines are shown in Fig. 2. Design equations for the ultimate shear strength of the joint panels and associated hysteresis models for 12 different details of RCS joints, including through-beam and through-column types, are included, which can be used in advanced analysis that considers the inelastic behaviour of beam-column joints.

A new through-column-type RCS joint in which a steel profile totally encased inside RC column is directly welded to the steel beam, is recently proposed within European RCFS project SMARTCOCO (SmartCOCO report 2013). With the steel profile fully encased into the RC column, this joint detail allows to have a larger force transmission region from steel beam to column compared to the classical RCS joints described in Fig. 2. An experimental study on cyclic behaviour of this joint conducted by Nguyen *et al*. (2017) showed that it can be used as dissipative element in ductility class medium structures. However, from the practical point of view this joint detail requires a complex set of stirrups in the connection zone because the stirrups have to pass through the steel beam. To overcome this practical difficulty, a novel through-column-type joint, in which an H steel profile covered by two supplementary plates totally embedded inside RC column is directly welded to the steel beam (see Fig. 3), is recently proposed within INSAR-UTC project (NAFOSTED 2016). The two supplementary plates are added to omit the stirrups resisting shear in the connection region. This kind of joint detail is not covered yet by the existing design guidelines. Indeed, Eurocodes 2, 3 and 4 give some provisions that can partly be used for the design of such a joint. There remains however a real lack of knowledge relatively to the issue of the force transmission from the embedded steel profile to the surrounding concrete of the column. Questions that can rise when designing such a connection are about the optimal anchorage length to embed the H steel profile or the optimal length of the supplementary plates. Therefore, experimental tests and numerical simulations need to be conducted to answer to these questions.

This paper presents an experimental investigation and modelling of the static behaviour of the through-column-type RCS joint described in Fig. 3. The first part of the paper is dedicated to present the testing of two full-scale through-column-type RCS joints under static loading. Next, a nonlinear 3D finite element model (FEM) is developed using ABAQUS software to predict the response and behaviour of the studied RCS joint. The FEM is then validated using the experimental results. An extensive parametric study was performed to investigate the influences of the stirrups, the encased profile length and supplementary plate length on the behaviour of the studied RCS joint.

2. Experimental study

2.1 Description of test specimens

Two full-scale through-column-type RCS joint specimens were tested at the Structure Laboratory of the University of Transport and Communication of Hanoi. The dimensions of the specimens are applicable to be used for construction medium-rise structural buildings. Fig. 4 shows the specimens' details. The specimens had the same size, geometry and material properties. The primary difference from one specimen to other was the presence of two supplementary plates wedded to embedded profile in the

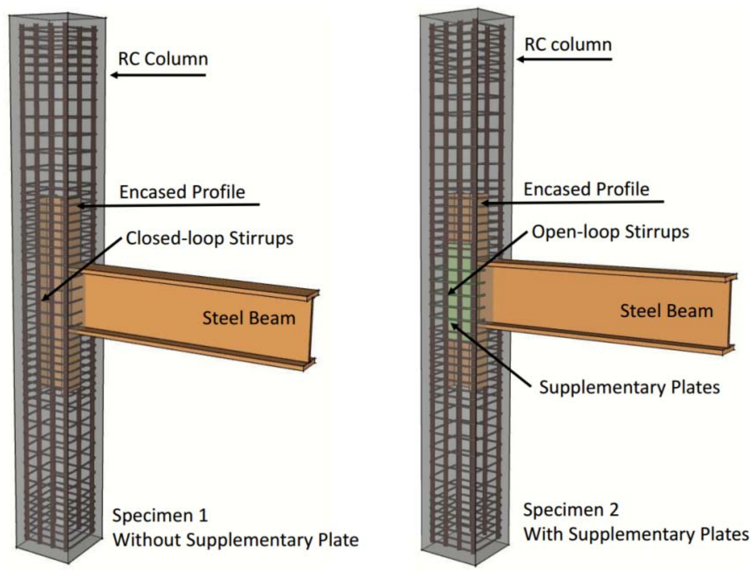

Fig. 3 Novel through-column-type joint detail proposed within INSAR-UTC project (2016-2019) (NAFOSTED 2016)

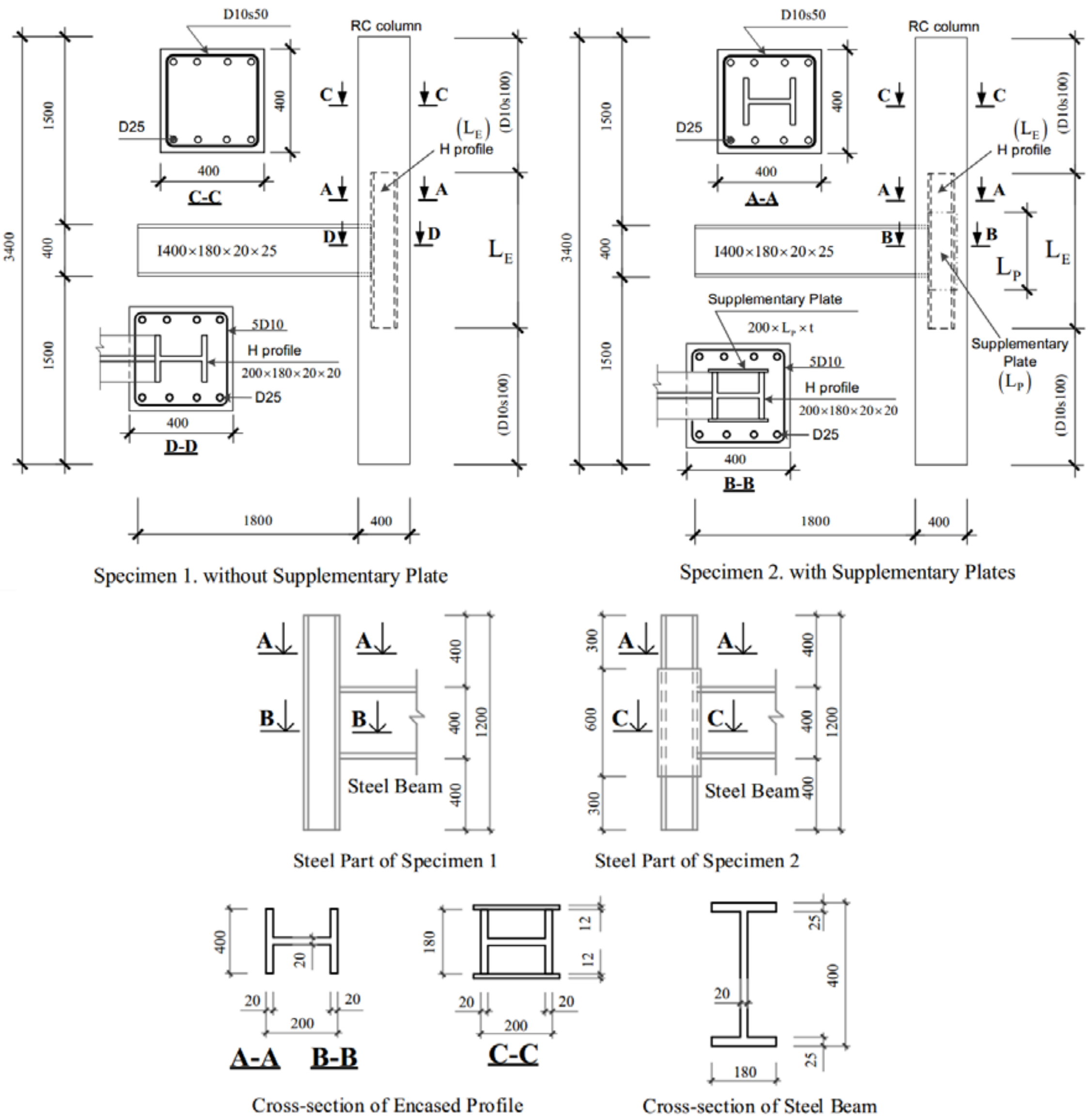

Fig. 4 Dimensions of the specimens joint specimen

connection region in order to pass over the stirrups passing through the steel beam. The specimens were designed according to Eurocode 4 (2004) and the tentative design method proposed within European RCFS project SMARTCOCO (2013). Both specimens consisted of 3 m height RC column with 40x40 cm^2 square cross-section reinforced by 8D25 longitudinal steel bars as shown in Fig. 4. D10 bars are used for shear reinforcement. The steel beam is 2m length with cross-section dimension shown in Fig. 4. The steel beam is welded to a H profile of 1.2 m length which is fully encased into the RC column. Compared to specimen 1, the specimen 2 had two supplementary plates wedded to the flanges of the H profile. The dimension of the H profile and the supplementary plates is indicated in Fig. 4. It is noted that the stirrups inside of the connection region of the specimen 1 were passed through 12 mm holes in the steel beam web in order to play the role of shear reinforcement, while in specimen 2 they were not. The stirrups were presents in the connection zone of the specimen 2 just for the structural reinforcement. Note that in order to evaluate the joint resistance and get the failure in joint region the steel beam has been oversized.

2.2 Material properties

The test specimen used normal weight concrete with a targeted 28 days concrete compressive strength of 45.6 MPa. The concrete compressive strength was determined based on the average value of compressive tests carried out on standard cylinders. At the day of testing of the specimen, the obtained average concrete compressive strength was about 46 MPa. The yield stress f_y and ultimate stress f_u for coupon tensile tests are reported for the structural reinforcing steel components in Table 3.

2.3 Test setup

The test setup is shown in Fig. 5. Specimens were loaded at the steel beam end by a hydraulic actuator of 1000 kN capacity with a stroke length of 150 mm. The actuator

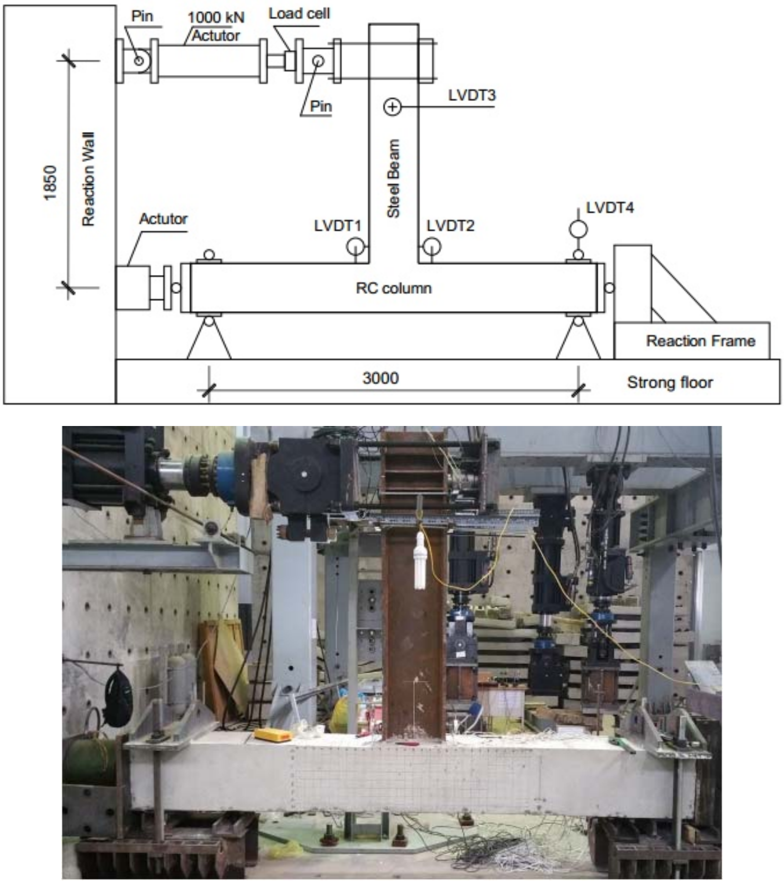

Fig. 5 Test setup

was operated in displacement control and horizontally held to the strong wall. A steel plate was used in the space between the specimen and the actuator for smooth transfer of actuator load at the column level. Furthermore, an axial load of 750 kN was applied at the top of the column. This load level which is maintained during the test, corresponds to about 10% of column load bearing capacity. Pinned boundary conditions at the each end of the columns were simulated by two supports as shown in Fig. 5. No restraint was provided against rotation along any axis. PTFE plates were placed between supports and specimen in order to avoid the friction and allow the specimen to deform freely in the horizontal direction. A transverse brace system was used in order to avoid out-of-plan displacement of the specimens.

2.4 Instrumentation

Several different instruments were used in the testing of the specimens. The arrangement of the instrumentation is presented in Fig. 6. During the loading, the test results were recorded every second. The data acquisition devices include:

- The 5 LVDT to measure displacement;
- 2 strain gauges rosettes placed in embedded profile to record the strains;
- 11 strain gauges placed in transverse and longitudinal reinforcements to record the strains.

2.5 Experimental results

2.5.1 General observations on the behavior of RCS joint

As a general observation in term of crack pattern, the two tested specimens had different behavior and faire mode. Two tests performed showed an expected behavior in accordance with the design process. The specimen 1 (without supplementary plates) was failed by panel shear at the connection zone while the specimen 2 (with supplementary plates wedded to the flanges of the encased profile) was failed by bending acting at the end of encased profile (Fig. 7). It should be noted that by adding the supplementary plates, the initial stiffness of Specimen 2 was marginally greater than that of Specimen 1 and the joint resisting bending moment increased about 15%. Note that the joint bending moment is calculated by multiplying the applied force with the distance between the loading point and the axis of the column.

The experimental observations at the characteristic points A, B, C and D of the load-drift curve are presented in Figs. 8-9.

The point A corresponds to the first crack appeared in column at the lower beam flange level. This crack is due to the local compression force resulting the transmission of the shear force of the beam to column. This crack was observed very early at about 0.5% drift for both specimens and their propagation was not significantly during the loading. Note

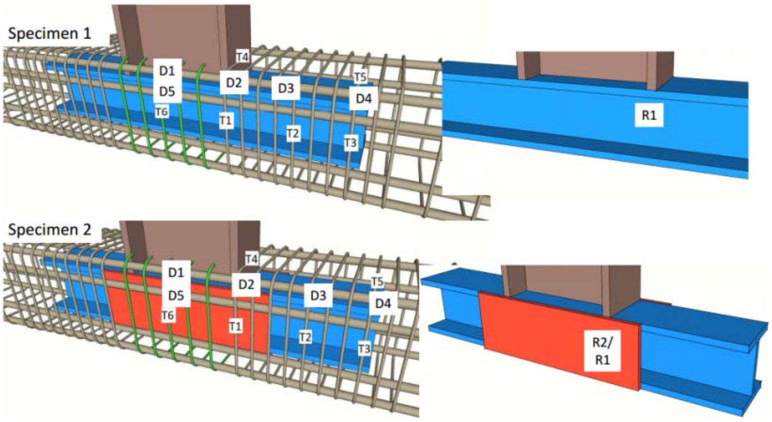

Fig. 6 Arrangement of measuring strain gauges and rosettes

that the drift of the specimen is calculated as the ratio of the total relative vertical displacement of the steel beam at the loading point with respect to the distance between this point and the axis of the column. The point B represents the first diagonal crack at the connection zone. This crack is caused by the shear and appeared approximately at 0.75% drift in specimen 1 and at 1.5% in specimen 2. However, it was observed that during the loading this crack propagated and opened much more in specimen 1 than the specimen 2. As can be seen from Fig. 8 the main diagonal cracks crossing the entire width of the specimen 1 from the bottom corner to the opposite side at approximate 45 degrees. The point C corresponds to the first vertical crack due to the bending caused by the force transfer from the encased profile to concrete outside of connection region. This crack appeared approximately at 1.25% drift in specimen 1 and at 0.75% in specimen 2. It was observed that the cracks due to bending propagated and opened much more in specimen 2 than the specimen 1.

Fig. 7 Cracking patterns at the end of loading

2.5.2 Comparison of the results of tested specimens

In the experiments, strains at different places on reinforcement bar, steel profiles and concrete were measured using strain gauges and rosettes. The position of strain gauges and the rosettes on rebars, steel profiles and supplementary plates of test specimens are shown in Fig. 6. The recorded strains were used to calculate the axial stress in rebar and the Von Mises stress in the steel in order to

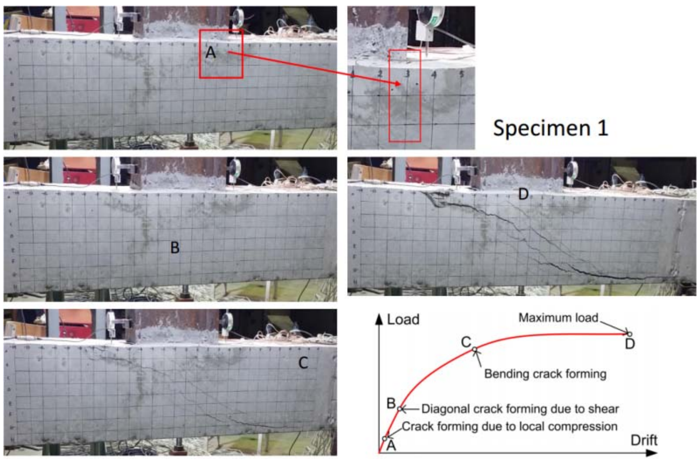

Fig. 8 Crack pattern of specimen 1

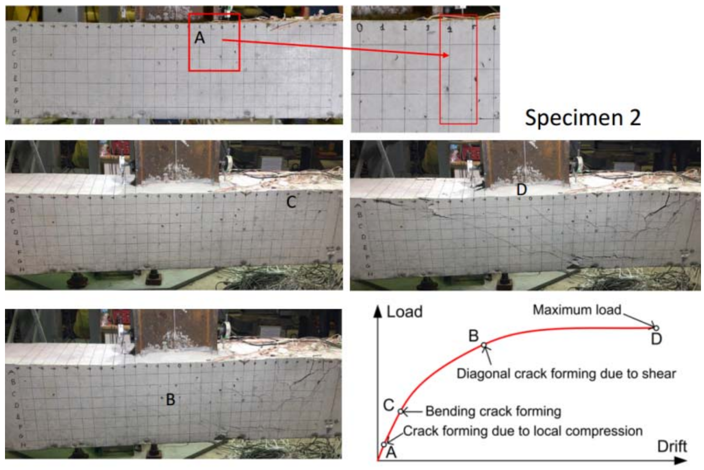

Fig. 9 Crack pattern of specimen 2

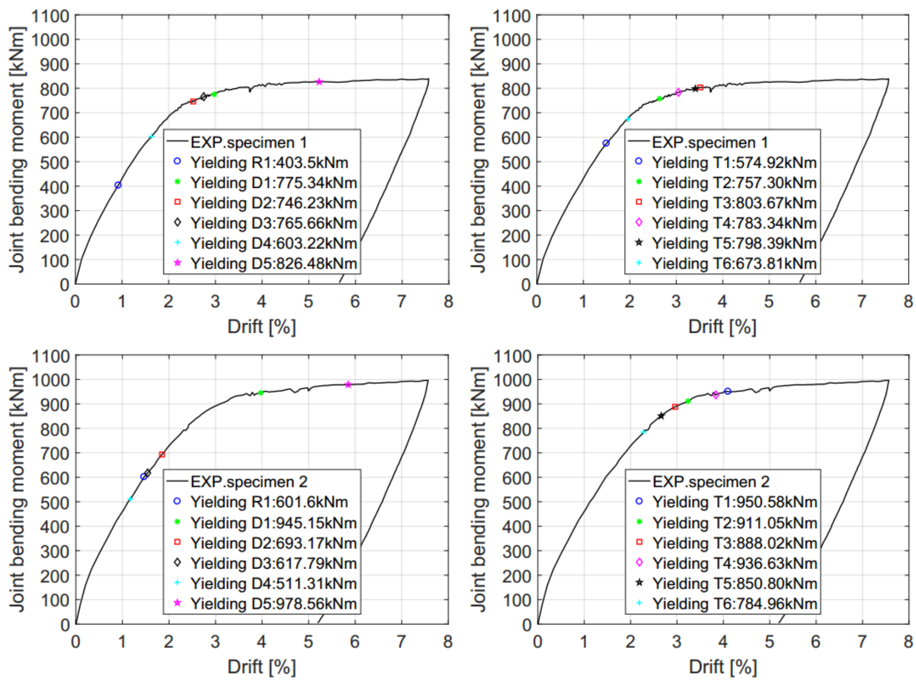

Fig. 10 Joint bending moment versus drift curves and yielding points

Table 1 Comparison of the yielding points between Specimen 1 and Specimen 2

Yielding at		T1	T2	T3	T4	T5	T6	R1	D1	D2	D3	D4	D5
Specimen 1	Drift (%)	1.5	2.64	3.52	3.05	3.41	1.96	0.92	2.98	2.53	2.75	1.63	5.23
	Moment (kNm)	574.92	757.3	803.67	783.34	798.39	673.81	403.5	775.34	746.23	765.66	603.22	826.48
Specimen 2	Drift (%)	4.1	3.24	2.96	3.84	2.66	2.28	1.47	3.98	1.85	1.54	1.17	5.85
	Moment (kNm)	950.58	911.05	888.02	936.63	850.8	784.96	601.56	945.15	693.17	617.79	511.31	978.56

estimate the applied load at which the steel reinforcement and profile start to be yielded. For the sake of simplicity, an elastic perfectly plastic behavior of steel is assumed.

The data collected from rosette R1 pointed out that the web of steel profile was yielded at about 0.9% and 1.4% drift for Specimen 1 and Specimen 2, respectively. It indicated that the steel profile had been reinforced considerably by supplementary plates. The data from strain gauges in column region (D2, D3 and D4) shown that the longitudinal reinforcement of Specimen 2 was yielded at lower applied load than that of Specimen 1 did. However, the reinforcement bar in joint region (strain gauge D1) was yielded at about 2.98% drift for Specimen 1 and 3.98% drift for Specimen 2. This fact was resulted from adding supplementary plates into Specimen 2 which helped to transfer the load more effectively from joint region to column and reduce the deformation in joint region. Consequently, the damages distribute from the joint region to column (see Fig. 7).

The joint bending moment and drift of Specimen 1 were presented in Fig. 10. By comparing the unit strains recorded from strain gauges and rosettes with the yielding limit of the reinforcement and structural steel, it was found that the first yielding, detected by Rosette R1, at the joint bending moment of 403.5 kNm, was at the web panel in shear. The yielding of strain gauge T1 appeared at the joint bending moment of 574.92 kNm, about 1.5% drift. The yielding of the stirrups was detected by the strain gauge T6 at the joint bending moment of 673.81 kNm. From this load level, Specimen 1 started to lose its stiffness. The yielding of the stirrups was detected by the strain gauge T2-T6 at the joint bending moment of 700 kNm to 800 kNm.

The behavior of Specimen 2 was notably different from that of Specimen 1 in terms of the yielding. Table 1 shows the comparison of drift and bending moment at different yielding points between Specimen 1 and Specimen 2. The yielding points are determined by the recorded data of the strain gauges and the rosettes. In fact, the first yielding of the longitudinal reinforcement in D4 was detected at the joint bending moment of 511.31 kNm. The yielding was found in tension of the web panel at the joint bending moment of 601.56 kNm (rosette R1). The yielding of the stirrups was detected by the strain gauge T6 at the joint bending moment of 784.96 kNm. From this load level, Specimen 2 started to lose its stiffness. From the bending moment of 850 kNm to 950 kNm, the yielding of the others was observed. Unlike Specimen 1, the last yielding of stirrups detected in position of strain gauge T1. The influence of the supplementary plates on the force transfer from steel beam to embedded profile was notable. It causes a decrease of the deformation in the interaction between beam and encased profile. The increasing stiffness of encased profile explains the yielding at strain gauge T1 was found later in Specimen 2 than Specimen 1. It shown that the force transfer from steel beam was displaced to column region (at the end of encased profile) and consequently the yielding of stirrups here (strain gauge T5) was detected early than it in Specimen 1.

3. Finite element model

3.1 General

Advances in computational features and software have brought the finite element method within reach of both academic research and engineers in practice by means of general-purpose nonlinear finite element analysis packages, with one of the most used nowadays being software (Abaqus 2013). The program offers a wide range of options regarding element types, material behaviour and numerical solution controls, as well as graphic user interfaces, auto-meshes, and sophisticated post-processors and graphics to speed the processing of the results. In this paper, this commercial software is employed to develop reliable three

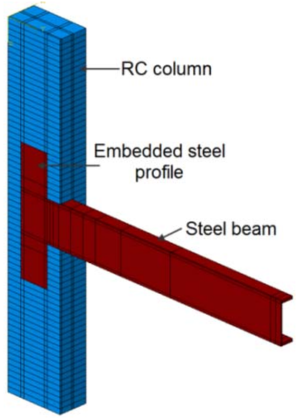

Fig. 11 Model of a half exterior RSC joint specimen

dimensional finite element model for the RCS joint specimen.

Due to the symmetry of the specimen geometry and loading, in order to save the calculation time, only half of the specimen was modelled. Fig. 11 shows the FE model for a half of the specimen. Five components of specimen (concrete column, rebars, steel beam, embedded steel H profile and supplementary plates) are modelled separately and assembled to make a complete specimen model. In addition, the interaction between components influences greatly the analysis results. Thus, the interface and contact between the concrete in joint region and the structural steel, the interaction of reinforcement and concrete need also to be modelled. Furthermore, the choice of element types, mesh sizes, boundary conditions and load applications that provide accurate and reasonable results are also important in simulating the behaviour of the RCS joint. Displacements are assumed to be small therefore the nonlinear geometric effect is not considered. However, the material nonlinearity is included in the finite element analysis.

3.2 The selection of element type and meshing

Fig. 12 presents the finite element type and mesh for all components of the specimen. In order to achieve the reliable results, the fine mesh was used in the connection zone. Reasonable convergence was achieved with such a mesh size, and refinement of the mesh was studied only up to the point where the change in the mesh size did not have an impact on the results. The concrete column and the steelwork part (beam, embedded profile and plates) are modelled with solid C3D8R element available in ABAQUS library. The C3D8R-element is an 8-node linear brick element with reduced integration stiffness and with hour-glass enhanced. Note that compared to the quadratic brick C3D20R element (20-node element), the accuracy of this element is slightly lower but using this element leads to a significant reduction of degree of freedom therefore computational cost. Furthermore, according to ABAQUS manual, this element is suitable for nonlinear analysis including contact, large deformation, plasticity, and failure. The reinforcement bars can be modelled using solid, beam or truss elements. The use of solid elements is computa-ionally expensive and therefore not chosen. Because the

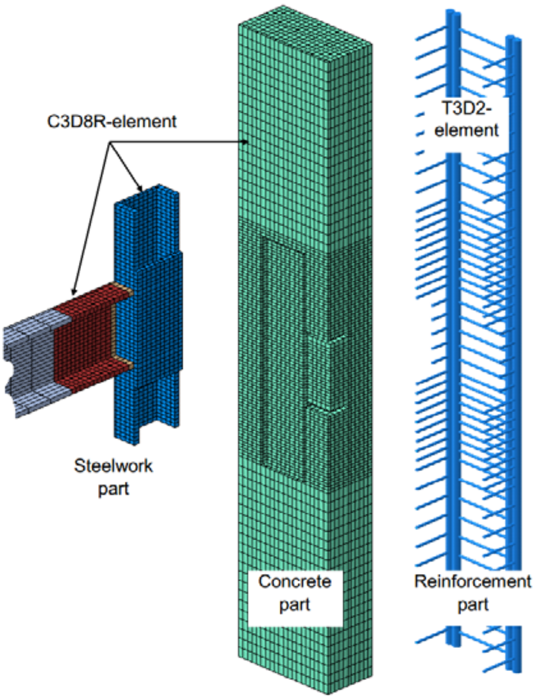

Fig. 12 FE type and mesh of components of the exterior RSC joint specimen

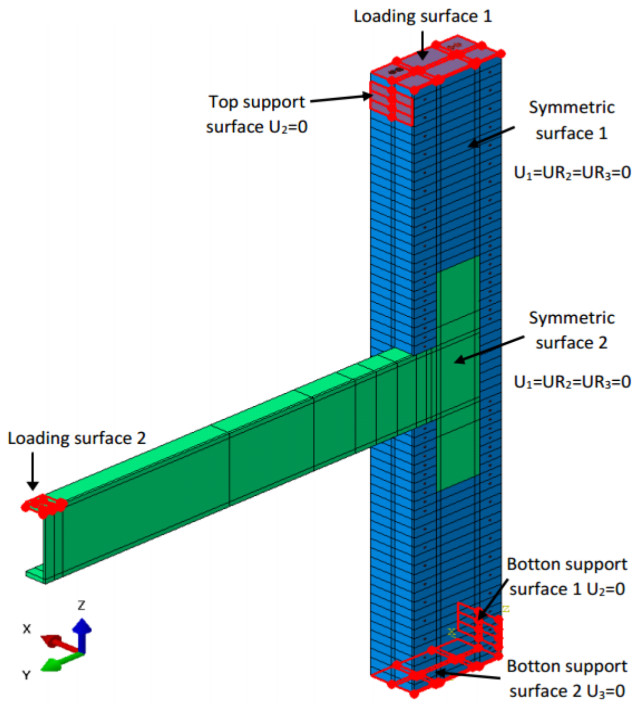

Fig. 13 Boundary conditions

reinforcing bars do not provide a very high bending stiffness, the 2-node linear 3-D truss elements, namely T3D2, are used.

3.3 Interaction conditions between components

Contact interactions between components may significantly affect the complete specimen behaviour and need to be carefully conditioned. In fact, the reinforcing bars are fully anchored in concrete so that embedded constraint can be used for the interaction between rebars and concrete surrounding. This constraint implies an infinite bond strength at the interface between the concrete and the reinforcement. In the present case, the truss elements representing the reinforcement are the embedded region while the concrete slab is the host region. Surface-to-surface contact elements (available in ABAQUS library) are used to model the interaction between concrete column and steel profile. The interaction properties are defined by the behaviour normal and tangential to the surfaces. For the normal behaviour, surface "hard" contact constraint is assumed. This type of normal behaviour implies that no penetration is allowed at each constraint location. For the tangential behaviour, the penalty frictional formulation is used and the coefficient of friction between the steel profile and the concrete column is assumed to be 0.5.

3.4 Boundary conditions and loadings

Boundary conditions that represent structural supports specify values of displacement and rotation variables at appropriate nodes. The boundary conditions for a half simulated specimen are illustrated in Fig. 13. The symmetry boundary condition is applied to the surfaces, which lies on the symmetric plane of the test specimen as identified by surfaces 1 and 2 in Fig. 13. These surfaces are taken as symmetric in the X-axis, which means that all nodes of the steel part (steel beam and embedded profile) and concrete column, which are located on these surfaces, are prevented from translating in the X direction, and rotating in Y and Z directions. The surfaces corresponding to the lateral supports on top and bottom of the RC column are restrained from moving in the horizontal direction (Y-axis) while the bottom surface of the RC column is restrained from moving in vertical direction (Z-axis). An axial force corresponding to 10% of column load bearing capacity is first applied to the column on surface 1 (see Fig. 13). Then, the applied axial force is maintained constant during the loading on loading surface 2 by displacement control.

3.5 Material modeling of concrete

The Concrete Damaged Plasticity (CDP) model, developed by Lee and Fenves (1998), available in ABAQUS material library is used to model the concrete material. This model consists of the combination of non-associated multi-hardening plasticity and scalar damaged elasticity to describe the irreversible damage that occurs during the fracturing process. The first parameter is the dilation angle which is measured at high confining pressure in the plan of hydrostatic pressure stress p and Von Mises equivalent stress q. The second parameter is the eccentricity of the plastic potential surface. The third parameter is the ratio of initial equibiaxial compressive yield stress $fb0$ to initial compressive yield stress $fc0$. The next parameter is named K which allows to determine the shape of loading surface in the deviator plane. The last one is the viscosity parameter which allows to slightly exceed the plastic potential surface area in certain sufficiently small problem

Table 2 Material parameter of CDP model for concrete of f_{cm} = 46 MPa

Density			**Parameters of CDP model**		
ρ (tonne/mm^3)	2.4×10^{-9}		Dilation angle	36^0	
Elasticity			Eccentricity	0.1	
E (Mpa)	33346		fb0/fc0	1.15	
υ	0.2		K	0.6667	
			Viscosity Parameter	0.0001	
Compressive behavior			**Tensile behavior**		
Yield stress (Mpa)	Inelastic strain	Damage	Yield stress (Mpa)	Displacement (mm)	Damage
18.4	0	0	3.34	0	0
31.83	0.00020	0.045	2.23	0.076	0.438
41.09	0.00049	0.101	1.50	0.141	0.710
46.00	0.00115	0.208	1.00	0.199	0.877
45.07	0.00152	0.269	0.68	0.253	0.981
42.22	0.00196	0.343	0.45	0.305	1.045
37.40	0.00244	0.432	0.30	0.354	1.086
27.78	0.00320	0.593	0.21	0.404	1.110

steps to overcome convergence problems. Therefore, a very small value (0.0001) is chosen for simulation in this study.

For compressive behaviour, the uniaxial stress-strain curve of Eurocode 2 (2004) is selected for the determination of yield stress and inelastic strain. The compressive stress is assumed to increase linearly with respect to the total strain until the initial yield/damage stress which is taken equal to 0.4*fm* where *fcm* is the mean compressive cylinder strength. The initial Young's modulus is calculated according to Eurocode 2 (2004). The Poisson's ratio is taken as 0.2. Then, the compressive stress grows until failure strength f_{cm}. The strain (ε_{c1}) associated with f_{cm} is equal to 0.0022, given by Eurocode 2 (2004). After exceeding the compression strain ε_{c1}, localization of damage occurs and the compressive stress decreases with the softening strain.

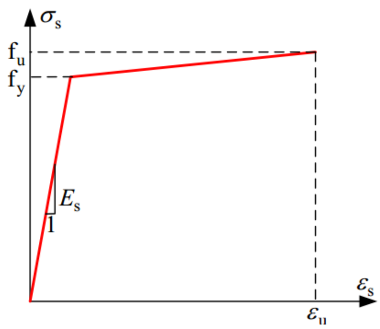

Fig. 14 Stress-strain relationship for the steel parts

For tensile behaviour of concrete, the effects of the reinforcement interaction with concrete are considered and the tension stiffening is specified by means of a post-failure stress-displacement relationship. As stated in the ABAQUS manual, in cases with little or no reinforcement, the stress-strain tension stiffening approach often causes mesh-sensitive results. Therefore, the fracture energy cracking criterion was used in this study. With this approach, the brittle behaviour of concrete is characterized by a stress-displacement response rather than a stress-strain response. The displacement is determined primarily by the crack opening, and it does not depend on the element length or the mesh size. The damage parameters in compression as in tension are determined by assuming that the split of inelastic strains into plastic and damaging parts by the scalar parameter as proposed by Kratzig and Polling (2004). The material properties assigned in CDP model are summarized in Table 2.

3.6 Material modeling of steel

The fracture model (Vasdravellis *et al*. 2014) checked through post-processing of the 3D stress and equivalent plastic strain. However, the stress-strain relationships obtained from the material tensile test were converted to piecewise bi-linear curve as shown in Fig. 14 and used for the modelling of the steel beam, the embedded profile, the

Table 3 Typical stress-strain properties of steel

Model	Steel beam	Embedded profile	Supplementary plate	Rebar	Stirrup
Modulus E_s (Gpa)	210	210	210	200	200
Yield stress f_y (Mpa)	305	305	305	435	520
Ultimate strength f_u (Mpa)	435	435	435	590	630
Ultimate strain	0.45	0.45	0.45	0.42	0.37

steel plates and the rebars. An elastoplastic model using Mises yield surface to define the isotropic hardening, available in ABAQUS material library, is adopted. The tangent hardening modulus being determined using the data presented in Table 3, in order to avoid numerical problems.

3.7 Validation of the FE model

In order to validate the accuracy of the FE model, the two test specimens were modelled. The results obtained in the numerical analysis, in terms of moment-drift responses were compared with the results obtained in the experimental tests in the same terms. As can be seen from Fig. 15, the numerical results are in good agreement with the experimental ones, both in terms of initial stiffness and ultimate bending moments. It can be noticed that the initial stiffness obtained in the numerical analysis is higher than the one obtained in the experimental tests. This difference appears due to the fixing set between the test specimen and the supports. If the results obtained in the numerical analysis and in the experimental tests are compared at the limit stage, it can be observed that the values of the ultimate forces and ultimate displacements are quite close for all tested elements. For the specimen without steel plate, the FE model predicts an ultimate joint bending moment of 841.8 kNm at 7% which is only 0.6% higher than the experimental value. Regarding the specimen with steel plate, the ultimate joint bending moment predicted by the FE model is about 1% greater than the experimental one. It should be noted that in the FE model it is assumed that the supplement steel places are perfectly welded on the embedded profile. However, after the test it was observed at the end that one steel plate was detached because of the failure of welded connection. It may explain the difference of the ultimate loads between the numerical and experimental results.

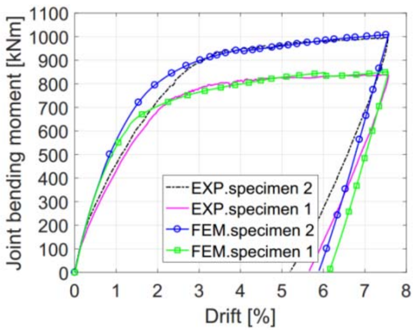

Fig. 15 Numerical-experimental comparison of joint bending moment versus drift

During the experimental tests, the strains at different point on rebars and on encased steel profile were measured using strain gauges and rosettes. The locations of the strain gauges, of the strain gauge rosettes are shown in Fig. 6. In order to know at what level of applied load the steel reinforcement and profile are yielded, the axial stress in rebars and the Von Mises stress in steel profile are

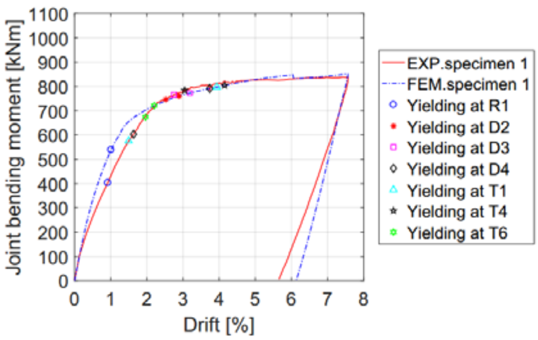

(a) Specimen 1

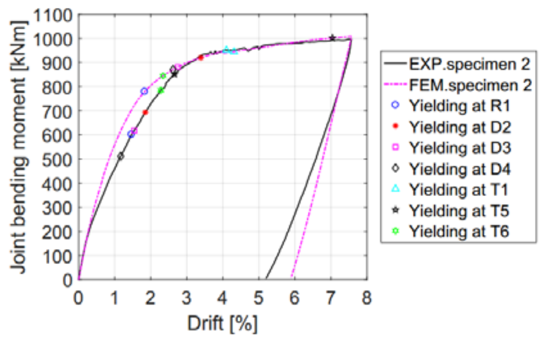

(b) Specimen 2

Fig. 16 Numerical-experimental comparison of yielding points

Table 4 Numerical-experimental comparison of yielding points

Specimen 1		**T1**	**T2**	**T3**	**T4**	**T5**	**T6**	**R1**	**D1**	**D2**	**D3**	**D4**
Exp.	Drift (%)	1.5	2.64	3.52	3.05	3.41	1.96	0.92	2.98	2.53	2.75	1.63
	Moment (kNm)	574.92	757.3	803.67	783.34	798.39	673.81	403.5	775.34	746.23	765.66	603.22
Model	Drift (%)	3.94	x	x	4.15	x	2.21	1.01	x	2.89	3.19	3.74
	Moment (kNm)	796.91	x	x	803.99	x	720.89	538.54	x	759.80	772.13	791.32
Specimen 2		**T1**	**T2**	**T3**	**T4**	**T5**	**T6**	**R1**	**D1**	**D2**	**D3**	**D4**
Exp.	Drift (%)	4.1	3.24	2.96	3.84	2.66	2.28	1.47	3.98	1.85	1.54	1.17
	Moment (kNm)	950.58	911.05	888.02	936.63	850.8	784.96	601.56	945.15	693.17	617.79	511.31
Model	Drift (%)	4.31	x	x	x	7.04	2.34	1.83	x	3.39	2.75	2.62
	Moment (kNm)	943.87	x	x	x	1001.4	844.71	779.41	x	919.43	881.35	870.8

Table 5 Set of parameters 1 for parametric study

Name of model / Parameter sets	Length of embedded H profile L_e mm	Supplementary plate			Stirrups in joint region
		Length L_P mm	With **200** mm	Thickness t_P mm	
L_e40	400				5D10 Closed-hoop Stirrups
L_e60	600				
L_e80	800				
L_e100	1000				
L_e120	1200				
L_e160	1600				
L_e200	2000				
L_e340	3400				
$L_e120L_P2\times15t_P1.2$	1200	2×150	200	12	5D10 Open-hoop Stirrups
$L_e120L_P30t_P1.2$	1200	300	200	12	
$L_e120L_P35t_P1.2$	1200	350	200	12	
$L_e120L_P40t_P1.2$	1200	400	200	12	
$L_e120L_P60t_P1.2$	1200	600	200	12	
$L_e120L_P80t_P1.2$	1200	800	200	12	
$L_e120L_P100t_P1.2$	1200	1000	200	12	
$L_e120L_P120t_P1.2$	1200	1200	200	12	
$L_e120L_P40t_P0.5$	1200	400	200	5	5D10 Open-hoop Stirrups
$L_e120L_P40t_P0.8$	1200	400	200	8	
$L_e120L_P40t_P1.0$	1200	400	200	10	
$L_e120L_P40t_P1.2$	1200	400	200	12	
$L_e120L_P40t_P1.8$	1200	400	200	18	

Table 6 Set of parameters 2 for parametric study

Name of model / Parameter sets	Length of embedded H profile L_e mm	Supplementary plate			Stirrups in joint region	Axial force (% column ultimate axial load)
		Length L_P mm	With **200** mm	Thickness t_P mm		
L_e120	1200				5D10 Closed-hoop Stirrups	0
L_e120.AF10	1200					10
L_e120.AF20	1200					20
L_e120.AF30	1200					30
L_e120.AF40	1200					40
L_e120.AF50	1200					50
L_e120.AF60	1200					60
L_e120.AF70	1200					70
$L_e120L_P60t_P1.2$	1200	600	200	12	5D10 Open-hoop Stirrups	0
$L_e120L_P60t_P1.2$AF10	1200	600	200	12		10
$L_e120L_P60t_P1.2$AF20	1200	600	200	12		20
$L_e120L_P60t_P1.2$AF30	1200	600	200	12		30
$L_e120L_P60t_P1.2$AF40	1200	600	200	12		40
$L_e120L_P60t_P1.2$AF50	1200	600	200	12		50
$L_e120L_P60t_P1.2$AF60	1200	600	200	12		60
$L_e120L_P60t_P1.2$AF70	1200	600	200	12		70

calculated using the recorded strains and the steel properties obtained from the standard tension test. Fig. 16 and Table 4 show the numerical-experimental comparisons in terms of local yielding points during the loading. Regarding the yielding of the embedded profile web in tension (Rosette R1), it can be found that the FE model predicts quite well the yielding of the embedded profile web in tension. However, as for the yielding of reinforcement the numerical results differ from experimental ones. This can be explained by the fact that the concrete was modelled by a continuous damage plasticity model and the reinforce-ment is assumed to be perfectly embedded in concrete. Indeed, the strain measured by strain gauge in rebars depends strongly on the crack pattern. Therefore, if a crack goes through the strain gauge position the measured strain in this case is much greater than the case without cracks.

4. Parametric study

Using the 3D FE model which was successfully validated against experimental results of the studied RCS joint, a set of parametric studies was undertaken to understand the behaviour of the joint as the components of the joint varied. The goal of this parametric study is to find out the configuration of the steel part that leads to the better performance of the beam-column joint. Therefore, the geometrical properties of the beam and the RC column (showed in Fig. 4) are unchanged. The behaviour of the joint is firstly investigated for the change of the length of encased H profile. Then, the influence of the length and the thickness of supplementary plates on the joint response is studied. Finally, the influence of the column axial force is investigated. The details of the parametric values considered are listed in Tables 5 and 6.

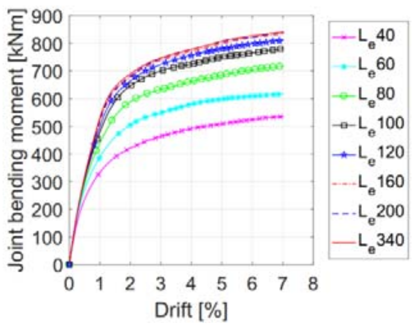

Fig. 17 Effect of encased profile length

4.1 Effect of encased profile length

The influence of length of encased H profile on the global behaviour of the hybrid joint is presented in Fig. 17 in term of moment-drift curves. The length of embedded H profile, namely L_e, was taken from 40 cm to 340 cm. It can be observed that, for L_e smaller than 120 cm, the stiffness and resistance of the joint increase with increasing of L_e. However, there is not a significant increasing in moment-drift behaviour when L_e cm. By looking at the evolution of the contact stress at the interface concrete/embedded profile, it has been seen for all considered cases of L_e that the force transmission took place in the joint zone whose length is less than 120 cm.

Fig. 18 and Table 7 shows the comparisons between model L_e60 and model L_e120 in terms of yielding points during the loading. One observes that in the model L_e60 the encased profile and the reinforcement are yielded more or less together at the bending moment level between 71% and 95.6% of the ultimate bending moment. In the model L_e120 the encased profile is yielded first at the bending moment level between 62% and 74% of the ultimate bending moment while the reinforcement is yielded separately at the bending moment level between 82% and 92% of the ultimate bending moment. It is to say that that the total anchorage length of the encased profile is more or less 120

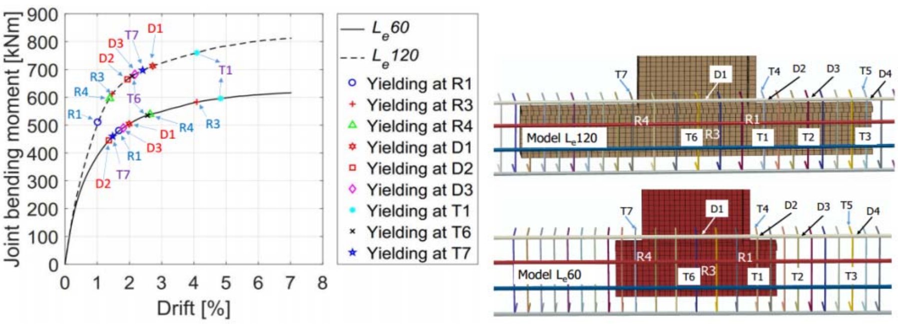

Fig. 18 Comparison between model L_e60 and model L_e120

Table 7 Comparison between model L_e60 and model L_e120

	Model	T1	T4	T6	T7	R1	R3	R4	D1	D2	D3	D4
L_e60	Drift (%)	4.83	4.63	2.56	1.48	1.68	4.09	2.64	1.99	1.36	1.81	x
	Moment (kNm)	595.89	590.89	535.24	459.93	479.43	583.49	539.09	504.13	445.30	477.13	x
L_e120	Drift (%)	4.09	x	2.08	2.41	1.02	1.46	1.39	2.72	1.94	2.17	2.13
	Moment (kNm)	759.8	x	708.94	696.17	509.86	612.17	595.89	712.4	664.58	682.65	679.69

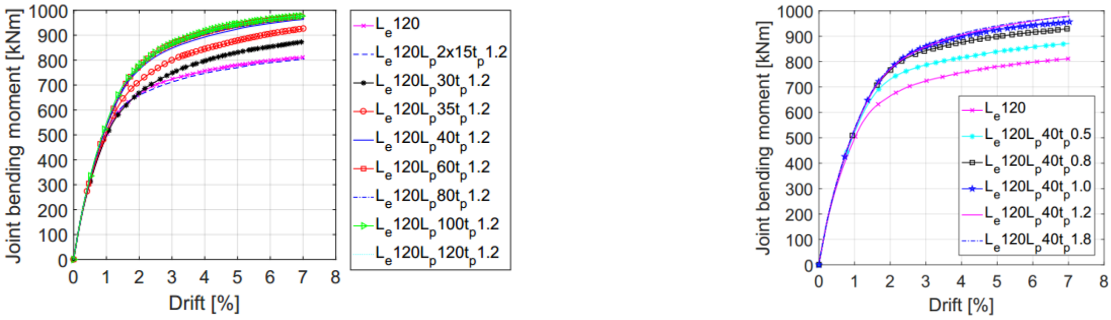

(a) influence of length (b) influence of thickness

Fig. 19 Effect of supplementary plates

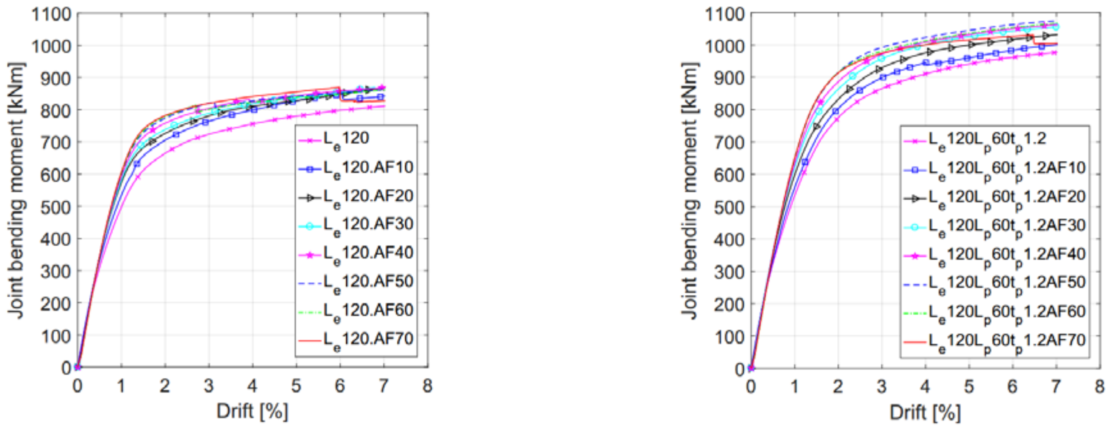

(a) Without supplementary plate (b) With supplementary plate

Fig. 20 Effect of the axial force on the behavior

cm. From this numerical parametric study, it can be pointed out that the joint behaviour is not affected by the length of encased H profile when the later exceeds three times of the beam height. In other words, the total anchorage length of the encased profile is equal to three times of the steel beam height. Further, experimental research needs to be conducted to confirm this.

4.2 Effect of supplementary plates

The main advantage of the proposed joint detail compared to the one proposed in European (SmartCOCO 2017) project is that the stirrups in the beam-column connection region can be omitted because of the presence of supplementary plates. Therefore, in this parametric study the influence of the supplementary plates on the behaviour of the proposed joint is carried out. Note that, even though there are the plates, the open-loop stirrups are present in the joint region as non-structural reinforcement in order to avoid the non-mechanical cracks. Fig. 19 presents the moment-drift curves obtained with different lengths and thickness of supplementary plates. Note that the length of encased H profile L_e was taken equal to 120 cm in order to avoid the influence of length of the encased H profile. The length of supplementary plates, namely L_p, was fixed equal to the height of the steel beam. The thickness of supplementary plates, namely t_p, was taken from 5 mm to 18 mm. The pink line in Fig. 19 corresponds to the case without supplementary plate but five stirrups D10 are present in the joint region. The other curves correspond to the cases where the closed-loop stirrups are replaced by the open-loop ones and the two supplementary plates are welded to the encased profile in the joint region. It can be seen that the supplementary plates can play the role of closed-loop stirrups in the joint region. As can be seen from Fig. 19(a), the moment-drift curves are unchanged when the length of the plates equal to the height of the steel beam, i.e. L_p = 40 cm. This value is therefore kept unchanged for the investigation of the influence of the thickness of supplementary plates (Fig. 19(b)). The joint strength increases with increasing of plate thickness. This is to say that the joint resistance is conditioned by the strength of the panels in shear in the joint region. The behaviour of the joint does not show significant change when the thickness exceeds a half of H profile web thickness ($t_p \geq 10$ mm).

4.3 Effect of axial force

The influence of the column compression force on the global behaviour of the hybrid joint is presented in Fig. 20 in term of moment-drift curves. The column axial force is varied from 0 to 70% of the plastic compression strength of the RC column. In this parametric study, the length of encased H profile L_e was taken equal to 120 cm, the length of supplementary plates L_p was taken equal to the height of the steel beam and the thickness of supplementary plates t_p was taken equal to 12 mm. The results shown in Fig. 20 demonstrate that the compression axial force increases the joint stiffness and strength. It may be explained by the fact that the compression force confines the concrete and somehow create a pre-stressing in the joint region. This leads indeed to a favourable effect on the joint stiffness and strength.

5. Conclusions

In this paper, an experimental and numerical investigation of the behavior of a novel type of exterior RCS joint subjected to static loading has been presented. The considered exterior RCS connection consists of an H steel profile covered by two supplementary plates totally embedded inside RC column directly welded to the steel beam. This type of beam-to-column joint has been recently proposed within INSAR-UTC project (NAFOSTED 2016) because it seems to presents some advantages compared to the existing RCS joint in term of resistance and construction methods. The experimental test aimed at investigating the influence of the supplementary plates on the behavior of the joint. It has been found that these plates can play the role of the stirrups in the joint region. A 3D finite element model has been created using ABAQUS software. This model takes into account the material nonlinearities, interaction and the contact between steel and concrete. Extensive parametric studies have been carried out to investigate the encased profile length, the supplementary plate length, the supplementary plate thickness and the column compression axial force on the behavior of the joint. The numerical results indicated that the effect of length of embedded H profile on the joint behavior is no longer significant when it exceeds about three times of the steel beam height. This is to say that the optimal anchorage length to embed the H steel profile is $L_e = 3H_{beam}$. It has been found that the column compression force has a favorable effect on the joint stiffness and strength. It has been observed that that the presence of the supplementary plates in the joint region can allow to remove the stirrups in this region. Furthermore, parametric study performed with different lengths of the supplementary plates pointed out that the supplementary plates are needed only in the beam-column connection area. However, future experimental research needs to be conducted to confirm this.

Acknowledgments

This research is funded by Vietnam National Foundation for Science and Technology Development (NAFOSTED) under grant number 107.01-2016.06.

References

Abaqus User's Manual V.6.13 (2013), Dassault Systems Simulation Corp.

ASCE Task Committee on Design Criteria for Composite Structures in Steel and Concrete, (1994), Guidelines for design of joints between steel beam and reinforced concrete columns; *J. Struct. Eng.*, **120**(8), 2330-2357.

Baba, N. and Nishimura, Y. (2000), "Stress transfer on through beam type steel beam-reinforced concrete column joints", *Proceeding of 6th International Conference on Steel-Concrete Composite Structures*, Los Angeles, CA, USA, pp. 753-760.

Bahman, F.A., Hosein, G. and Nima, T. (2012), "Seismic performance of composite RCS special moment frames", *KSCE J. Civil Eng.*, **2**(2), 450-457. https://doi.org/10.1007/s12205-013-1431-5

Cheng, C.T. and Chen, C.C. (2005), "Seismic behavior of steel beam and reinforced concrete column connections", *J. Constr. Steel Res.*, **61**(5), 587-606. https://doi.org/10.1016/j.jcsr.2004.09.003

Deierlein, D.D. and Noguchi, H. (2004), "Overview of US–Japan research on the seismic design of composite reinforced concrete and steel moment frame structures", *J. Struct. Eng.*, **130**(2), 361-367. https://doi.org/10.1061/(ASCE)0733-9445(2004)130:2(361)

Deierlein, G.G., Sheikh, T.M., Yura, J.A. and Jirsa, J.O. (1989), "Beam-column moment connections for composite frames: Part 2", *J. Struct. Eng.*, **115**(11), 2877-2896. https://doi.org/10.1061/(ASCE)0733-9445(1989)115:11(2877)

Eurocode 2 (1992), EN1992-1-1 Design of concrete structures - Part 1: General rules and rules for buildings.

Eurocode 4 (1994), EN1994-1-1 Design of composite steel and concrete structures - Part 1: General rules and rules for buildings.

Fargier-Gabaldon, L. (2005), "Design of moment connections for composite framed structures", Ph.D. Dissertation; The University of Michigan, MI, USA.

Griffis, L.G. (1986), "Some design considerations for composite-frame structures", *Eng. J.*, **23**(2), 59-64.

Hui, M., Sanzhi, L., Zhe, L., Yunhe, L., Jing, D. and Peng, Z. (2018), "Shear behavior of composite frame inner joints of SRRC column-steel beam subjected to cyclic loading", *Steel Compos. Struct., Int. J.*, **27**(4), 495-508. http://dx.doi.org/10.12989/scs.2018.27.4.495

Kanno, R. and Deierlein, D.D. (1993), "Strength, deformation, and seismic resistance of joints between steel beams and reinforced concrete columns", Structural Engineering Report; No. 93-6, Cornell University, NY, USA.

Kanno, R. and Deierlein, D.D. (1996), "Seismic behavior of composite (RCS) beam-column joint assemblies", *Proceeding of Composite Construction in Steel and Concrete III*, Irsee, Germany, pp. 236-249.

Kanno, R. and Deierlein, D.D. (2002), "Design Model of Joints for RCS Frames", *Proceeding of Composite Construction in Steel and Concrete IV*, Alberta, Canada, pp. 947-958.

Kratzig, W.B. and Polling, R. (2004), "An elasto-plastic damage model for reinforced concrete with minimum number of material parameters", *Comput. Struct.*, **82**(15), 1201-1215. https://doi.org/10.1016/j.compstruc.2004.03.002

Lee, J. and Fenves, G.L. (1998), "Plastic-damage model for cyclic loading of concrete structures", *J. Eng. Mech.*, **124**(8), 892-900.

Li, W., Li, Q-N., Jiang, W-S. and Jiang, L. (2011), "Seismic performance of composite reinforced concrete and steel moment frame structures – state-of-the-art", *Compos. Part B: Eng.*, **42**(2), 190-206. https://doi.org/10.1061/(ASCE)0733-9399(1998)124:8(892)

Li, W., Li, Q.N. and Jiang, W.S. (2012), "Parameter study on composite frames consisting of steel beams and reinforced concrete columns", *J. Constr. Steel Res.*, **77**(10), 145-162. https://doi.org/10.1016/j.jcsr.2012.04.007

Men, J., Zhang, Y., Guo, Z. and Shi, Q. (2015a), "Experimental research on seismic behavior of a composite RCS frame", *Steel*

Compos. *Struct*., *Int*. *J*., **18**(4), 971-983. http://dx.doi.org/10.12989/scs.2015.18.4.971

Men, J., Guo, Z. and Shi, Q. (2015b), "Experimental research on seismic behavior of novel composite RCS joints", *Steel Compos*. *Struct*., *Int*. *J*., **19**(1), 209-221. https://doi.org/10.12989/scs.2015.19.1.209

Mohammad, H., Mohammad, R., Karim, A. and Hassan, A. (2013), "3D finite element modelling of composite connection of RCS frame subjected to cyclic loading", *Steel Compos*. *Struct*., *Int*. *J*., **15**(3), 281-298. https://doi.org/10.12989/scs.2013.15.3.281

NAFOSTED (2016), Experimental and numerical investigation on seismic behavior of composite reinforced concrete and steel joints; The National Foundation for Science and Technology Development, Vietnam.

Nguyen, X.H., Nguyen, Q-H., Le, D.D. and Mirza, O. (2017), "Experimental Study on Seismic Performance of New RCS Connection", *Structures*, **9**, 53-62. https://doi.org/10.1016/j.istruc.2016.09.006

Nishiyama, I., Kuramoto, H. and Noguchi, H. (2004), "Guidelines: seismic design of composite reinforced concrete and steel buildings", *J. Struct*. *Eng*., **130**(2), 336-342. https://doi.org/10.1061/(ASCE)0733-9445(2004)130:2(336)

Noguchi, H. and Kim, K. (1998), "Shear strength of beam-to-column connections in RCS system", *Proceedings of the Structural Engineers World Congress*, San Francisco, CA, USA.

Saeedeh, G., Ali, K., Meissam, N., Seyed, M. and Majid, G. (2016), "Nonlinear behavior of connections in RCS frames with bracing and steel plate shear wall", *Steel Compos*. *Struct*., *Int*. *J*., **22**(4), 915-935. http://dx.doi.org/10.12989/scs.2016.22.4.915

Sheikh, T.M., Yura, J.A. and Jirsa, J.O. (1987), "Moment Connections between Steel Beams and Concrete Columns", PMFSEL Report No. 87-4; University of Texas at Austin, Austin, TX, USA.

Sheikh, T.M., Deierlein, G.G., Yura, J.A. and Jirsa, J.O. (1989), "Beam-column moment connections for composite frames: Part 1", *J. Struct*. *Eng*., **115**(11), 2858-2876. https://doi.org/10.1061/(ASCE)0733-9445(1989)115:11(2858)

SMARTCOCO (2017), Smart Composite Components: Concrete Structures Reinforced by Steel Profiles – Final Report: European Committee: Research Programme of the Research Fund for Coal and Steel.

Vasdravellis, G., Karavasilis, T.L. and Uy, B. (2014), "Design rules, experimental evaluation, and fracture models for high-strength and stainless-steel hourglass shape energy dissipation devices", *J. Struct*. *Eng*., **140**(11). https://doi.org/10.1061/(ASCE)ST.1943-541X.0001014

BU